Inorganic Chemistry

Forum Article

pubs.acs.org/IC

Synthesis and Photophysical Study of a [NiFe] Hydrogenase Biomimetic Compound Covalently Linked to a Re-diimine Photosensitizer

Peter A. Summers,[†,‡] James A. Calladine,[†] Fabio Ghiotto,[†] Joe Dawson,[†] Xue-Z. Sun,[†] Michelle L. Hamilton,[†,§] Michael Towrie,[∥] E. Stephen Davies,[†] Jonathan McMaster,*[,†] Michael W. George,*[,†,‡] and Martin Schröder*[,†,⊥]

[†]School of Chemistry, The University of Nottingham, University Park, Nottingham NG7 2RD, United Kingdom

[‡]Department of Chemical and Environmental Engineering, The University of Nottingham Ningbo China, Ningbo 315100, China

[§]Dynamic Structural Science Consortium, Research Complex at Harwell, Didcot, Oxfordshire OX11 0FA, United Kingdom

[∥]Central Laser Facility, Research Complex at Harwell, Science and Technology Facilities Council, Rutherford Appleton Laboratory, Harwell Oxford, Didcot, Oxfordshire OX11 0QX, United Kingdom

[⊥]School of Chemistry, University of Manchester, Manchester M13 9PL, United Kingdom

Supporting Information

ABSTRACT: The synthesis, photophysics, and photochemistry of a linked dyad ([Re]-[$NiFe_2$]) containing an analogue ([$NiFe_2$]) of the active site of [NiFe] hydrogenase, covalently bound to a Re-diimine photosensitizer ([Re]), are described. Following excitation, the mechanisms of electron transfer involving the [Re] and [$NiFe_2$] centers and the resulting decomposition were investigated. Excitation of the [Re] center results in the population of a diimine-based metal-to-ligand charge transfer excited state. Reductive quenching by NEt_3 produces the radically reduced form of [Re], $[Re]^-$ ($k_q = 1.4 \pm 0.1 \times 10^7$ M^{-1} s^{-1}). Once formed, $[Re]^-$ reduces the [$NiFe_2$] center to $[NiFe_2]^-$, and this reduction was followed using time-resolved infrared spectroscopy. The concentration dependence of the electron transfer rate constants suggests that both inter- and intramolecular electron transfer pathways are involved, and the rate constants for these processes have been estimated ($k_{inter} = 5.9 \pm 0.7 \times 10^8$ M^{-1} s^{-1}, $k_{intra} = 1.5 \pm 0.1 \times 10^5$ s^{-1}). For the analogous bimolecular system, only intermolecular electron transfer could be observed ($k_{inter} = 3.8 \pm 0.5 \times 10^9$ M^{-1} s^{-1}). Fourier transform infrared spectroscopic studies confirms that decomposition of the dyad occurs upon prolonged photolysis, and this appears to be a major factor for the low activity of the system toward H_2 production in acidic conditions.

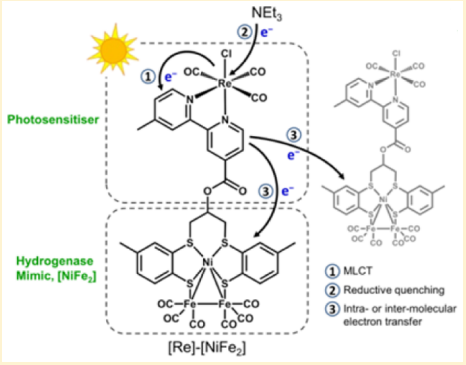

INTRODUCTION

There is increasing research interest in the area of solar fuels driven by growing global issues centered around the supply and demand of depleting energy resources.[1] Solar fuels provide the potential to convert solar energy into stored energy with applications in transportable fuels and chemical feedstocks. There are several strategies to achieve this including the photocatalytic splitting of water for the production of dihydrogen (H_2)[2] and the reduction of carbon dioxide (CO_2).[3] Traditionally, photochemical H_2 production has been achieved through the use of a photosensitizer (PS) and a sacrificial electron donor coupled with a catalyst able to reduce protons to H_2 (Scheme 1). In this scheme the absorption of light by PS generates an excited state (PS*), which can be reduced by a suitable electron donor (ED) to form the reduced photosensitizer, PS^-. Electron transfer to the catalyst then generates the intermediates required for the catalytic reduction of protons. Of particular note in this area was the recent work from Eisenberg and co-workers, who used a heterogeneous CdSe nanocrystal PS to deliver electrons to a nickel-based homogeneous catalyst in water, resulting in continuous H_2 production with little drop in activity over 360 h of photocatalysis.[4] In addition to the bimolecular systems described in Scheme 1, photosensitizing units have been successfully linked to catalysts and electron acceptors in an effort to facilitate and direct electron transfer and control charge recombination.[2b,5] Research into the utilization of homogeneous photocatalytic systems continues to be investigated widely, and a range of biomimetic catalysts, inspired by the active sites of the hydrogenases, have been studied.[2b,6]

Special Issue: Small Molecule Activation: From Biological Principles to Energy Applications Part 3

Received: July 31, 2015
Published: November 25, 2015

DOI: 10.1021/acs.inorgchem.5b01744
Inorg. Chem. 2016, 55, 527−536

Scheme 1. Simplified Schematic of the One-Electron Reduction of a Catalyst ([Cat]) by a Photosensitiser ([PS]) Proceeding via the Reductive Quenching of [PS]* by an Electron Donor (ED)

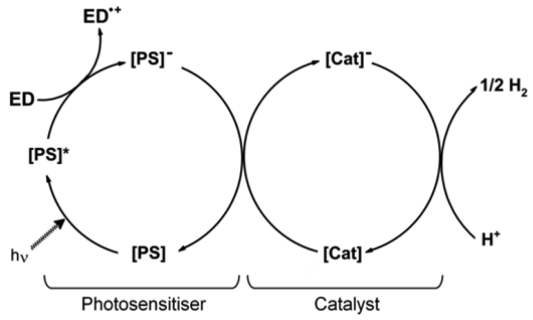

These enzymes are naturally occurring catalysts for the interconversion of protons and H_2, with high turnover efficiency at nearly neutral pH in aqueous environments.[7] Synthetic efforts have focused on the active sites of the [FeFe] hydrogenase with complexes such as $[Fe_2(CO)_4X(L^1)(L^2)]$ (where X is a dithiolate bridge, and L^1 and L^2 are either carbonyl or phosphine derived ligands) acting as the catalytic center, with Ru-, Ir-, or Re-derived photosensitizers.[8] The ground state and excited-state properties of [FeFe] hydrogenase model compounds have been studied in detail using a range of IR spectroscopies at a variety of excitation wavelengths. Following excitation, CO loss with geminate or diffusion recombination, as well as photoproducts assigned to the breaking and recombination of the Fe−Fe bond, have been observed.[9] Photosensitizing units have been attached directly to the [FeFe] units, either covalently through a dithiolate bridge integral to the [FeFe] complex or through ligand substitution reactions at the [FeFe] center.[10]

Steady-state and time-resolved spectroscopic studies have probed the photocatalytic mechanisms in linked and bimolecular systems, focusing on electron transfer to the catalyst.[10g,j,11] Transient absorption (TA) spectroscopy has monitored electron transfer in bimolecular systems from photogenerated $[Ru(bpy)_3]^+$ to $[Fe_2(CO)_4X(L^1)(L^1)]$ in CH_3CN (X = $(\mu$-$SCH_2)_2CH_2$, $L^1 = L^2 = CO$; X = $(\mu$-$SCH_2)_2NCH_2C_6H_5$, $L^1 = L^2 = CO$ or $L^1 = L^2 = P(Pyr)_3$ or $L^1 = CO$ $L^2 = P(Pyr)_3$; X = μ-Cl_2bdt^{2-}, $L^1 = L^2 = CO$; Pyr = N-pyrrolyl; bdt^{2-} = 3,6-dichlorobenzene-1,2-dithiolate).[8a,10g,11a] Time-resolved measurements have also been used to study electron transfer in linked systems. TA spectroscopy was used to observe electron transfer in a self-assembled system consisting of an [FeFe] hydrogenase mimic functionalized with a pendant pyridine group, linked to a zinc porphyrin photosensitizer.[10g] Similarly, TA spectroscopy has been used to study a zinc porphyrin covalently linked to an [FeFe] hydrogenase model complex, where rapid electron transfer from the zinc porphyrin to the catalyst was monitored (τ = 24 ± 1 ps) followed by charge recombination (τ = 57 ± 1 ps) in CH_2Cl_2.[10j] Time-resolved infrared (TRIR) spectroscopy was used to examine electron transfer in the analogous self-assembled system. Again, electron transfer from the photoexcited porphyrin to the catalyst was observed (τ = 40 ± 3 ps) with charge recombination (τ = 205 ± 14 ps) significantly slower than in the covalently linked system (τ = 57 ± 1 ps).[11b] However, turnover numbers (TON) in linked systems are generally lower or comparable to the analogous bimolecular, or separated, systems.[2b] For example, in a linked dyad containing an iridium-based cyclometalated photosensitizer covalently linked to an [FeFe] hydrogenase mimic, a maximum TON of 127 was reported, which is similar to the analogous separated system (TON = 138).[10m]

We recently reported a detailed mechanistic study into photocatalytic H_2 production from an bimolecular system using the photosensitizer $[ReCl(CO)_3(bpy)]$ and the catalyst $[NiFe_2]$ (Figure 1), an analogue of the active site of the

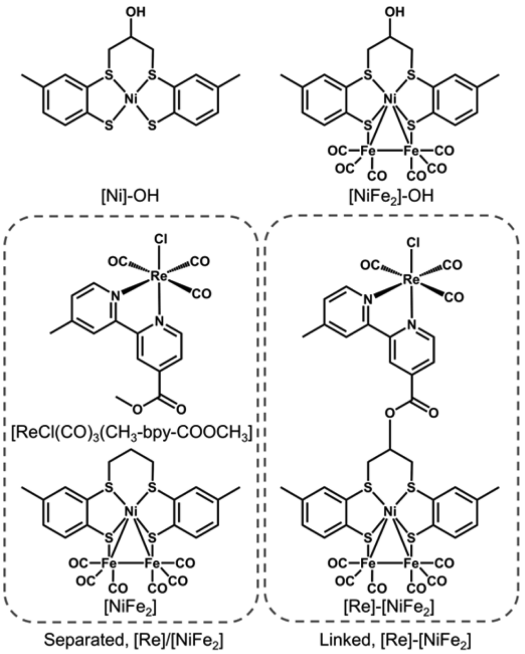

Figure 1. Structures of $[NiFe_2]$, $[NiFe_2]$−OH, $[ReCl(CO)_3(CH_3$-bpy-COOR)] (R = H or CH_3), and [Re]-$[NiFe_2]$.

[NiFe] hydrogenase,[12] which catalyzes H_2 production. In this paper we report the synthesis of a linked dyad containing a Re diimine based photosensitizer covalently linked to $[NiFe_2]$, [Re]-$[NiFe_2]$ (Figure 1). We investigate the photophysical properties of [Re]-$[NiFe_2]$ and monitor excited state formation, electron transfer processes and H_2 production. We compare the results for [Re]-$[NiFe_2]$ with an analogous bimolecular system, [Re]/$[NiFe_2]$ (a mixture of $[ReCl(CO)_3(CH_3$-bpy-$COOCH_3)]$ and $[NiFe_2]$, Figure 1) to evaluate the effects of covalently linking the [Re] and $[NiFe_2]$ units together and to provide valuable insight for the development of similar catalytic systems.

EXPERIMENTAL SECTION

General Procedures. Reagents were used as received from the suppliers (Sigma-Aldrich, Acros Organic, and Fluka), and all the reactions, manipulations, and transfers were performed under Ar using standard Schlenk techniques, unless stated otherwise. For TRIR, luminescence, and H_2 production experiments, acetonitrile (99.9%, Merck) and NEt_3 (>99.5%, Sigma-Aldrich) were distilled under an inert atmosphere of Ar from CaH_2. For electrochemical measurements, CH_2Cl_2 was dried, degassed, and stored under Ar. Trifluoroacetic acid (TFA) and $CDCl_3$ were degassed with Ar, stored over 4 Å molecular sieves, and used without further purification. N-$(CH_2CH_2OH)_3$ (TEOA; 98%, Alfa Aesar) was dried under reduced pressure (160 °C, 1×10^{-1} mbar) for 24 h before being stored under Ar. High-purity Ar was obtained from BOC. $[ReCl(CO)_3(bpy)]$,[13] $[NiFe_2]$ (Figure 1),[14] $[ReCl(CO)_3(CH_3$-bpy-COOH)][15] (CH_3-bpy-

DOI: 10.1021/acs.inorgchem.5b01744
Inorg. Chem. 2016, 55, 527−536

COOH = 4′-methyl-2,2′-bipyridine-4-carboxylic acid) and [ReCl(CO)$_3$(CH$_3$-bpy-COOCH$_3$)][16] (Figure 1, CH$_3$-bpy-COOCH$_3$ = 4′-methyl-2,2′-bipyridine-4-carboxylate) were prepared according to adapted literature methods. Elemental analyses were performed by the London Metropolitan University (Carlo Erba CE1108 Elemental Analyzer). NMR spectra were recorded on a Brüker DPX 300 spectrometer running at 300.13 MHz for ^{1}H and at 75.42 MHz for ^{13}C experiments. Electrospray (ES) mass spectrometric data were recorded by the Mass Spectrometry Service at the University of Nottingham using a Brüker Daltonics microTOF Electrospray Mass Spectrometer. X-band electron paramagnetic resonance (EPR) spectra were recorded on a Brüker EMX spectrometer. Simulations of EPR spectra were performed using the Brüker WINEPR SimFonia package.[17] FTIR spectra were recorded in solution cells (Harrick Scientific Products, Inc.) with CaF$_2$ windows using a Nicolet 6700 FTIR spectrometer, typically at 2 cm^{-1} resolution. Path lengths of 0.25, 0.39, 0.5, or 1 mm were used, and all solutions were prepared under an inert atmosphere of Ar and degassed by three freeze−pump−thaw cycles.

[Ni]−OH. NaOMe (0.359 g, 6.64 mmol) was added to a solution of toluene-3,4-dithiol (TDT; 0.520 g, 3.32 mmol) in anhydrous MeOH (30 cm^3) under Ar. The pink solution was stirred for 1 h before dropwise addition of a concentrated solution of [Ni(OAc)$_2$.4(H$_2$O)] (0.414 g, 1.66 mmol) in MeOH (10 cm^3). The dark brown solution was stirred for 1 h, after which time a concentrated solution of 1,3-dibromopropan-2-ol (0.542 g, 2.49 mmol) in MeOH (10 cm^3) was added. The reaction mixture was stirred for 24 h at room temperature, after which time a light green precipitate formed. The powder was collected by filtration and washed with cold anhydrous MeOH (2 × 5 cm^3) and anhydrous isohexane (3 × 5 cm^3) and dried in vacuo. Chromatography of the crude material on silica gel (Fluka, F60) using CH$_2$Cl$_2$ as eluent yielded one mobile colored fraction, which was isolated. Evaporation of this solution to dryness yielded a light green powder, [Ni]−OH. Yield 0.485 g, 69%. Elemental Analysis: Found (Calculated for C$_{17}$H$_{18}$O$_1$S$_4$ Ni$_1$) C, 48.53 (48.01); H, 4.63 (4.27)%. MS (ES$^+$) *m/z*: 425 (M + H)$^+$, 447 (M + Na)$^+$. ^{1}H NMR (300 MHz, deuterated dimethyl sulfoxide (DMSO-d_6), 298 K): δ_H 7.38−6.82 (6H, m, Ph-H), 4.81 (1H, s, OH), 3.94−3.92 (1H, m, CH), 3.83−3.50 (4H, m, SCH$_2$), 2.23 (6H, s, Ph−CH$_3$) ppm. ^{13}C NMR (75 MHz, DMSO-d_6, 298 K): δ_C 132.68−124.50 (m, Ph-C), 64.12 (s, C-O), 37.27 (s, SC), 20.92−20.36 (m, Ph-CH$_3$) ppm. IR (solid): 3260 (s), 2919 (s), 2863 (s), 2153 (w), 2011 (w), 1715 (s), 1606 (s), 1579 (s), 1512 (m), 1460 (vs), 1377 (s), 1326 (m), 1280 (s), 1253 (vs), 1196 (m), 1169 (s), 1111 (vs), 1044 (vs), 866 (s), 802 (vs), 772 (m), 689 (m), 638 (m), 577 (w), 563 (w), 535 (s), 521 (vs) cm^{-1}.

[NiFe$_2$]−OH. A mixture of [Ni]−OH (0.301 g, 0.73 mmol) and Fe$_3$(CO)$_{12}$ (0.339 g, 0.67 mmol) in anhydrous CH$_2$Cl$_2$ (40 cm^3) was heated to reflux for 16 h under Ar. The reaction mixture was subsequently cooled to room temperature, and the dark brown/red solution was filtered to remove a dark brown precipitate. The precipitate was washed with CH$_2$Cl$_2$ (3 × 5 cm^3), and the washings were combined with the filtrate. Concentration of the filtrate under reduced pressure afforded a dark brown solid, which was washed with anhydrous isohexane (3 × 5 cm^3) and dried in vacuo. Chromatography of the crude material on silica gel (Fluka, F60) using ethyl acetate and petroleum ether (bp 60−80 °C; 3/2, v/v) as eluent yielded two fractions. A fast-moving weak orange band was identified as [Fe$_2$(CO)$_6$TDT], an analogue of [Fe$_2$(CO)$_6$BDT] (BDT^{2-} = benzene-1,2-dithiolate) previously reported by Perra et al.[18] The second slow-moving brown band was isolated, and removal of the solvent under reduced pressure afforded a black powder, the target complex [NiFe$_2$]−OH. Yield 0.293 g, 62%. Elemental Analysis: Found (Calculated for C$_{23}$H$_{18}$O$_7$S$_4$Ni$_1$Fe$_2$) C, 39.98 (39.12); H, 3.12 (2.57)%. MS (ES$^+$) *m/z*: 727 (M + Na)$^+$. ^{1}H NMR (400 MHz, CDCl$_3$, 298 K): δ_H 8.17−7.20 (6H, m, Ph-H), 3.89−3.84 (1H, m, CH), 3.74 (1H, m, SCH$_2$), 3.38−3.31 (1H, m, SCH$_2$), 2.99−2.79 (2H, m, SCH$_2$), 2.58−2.49 (6H, s, Ph−CH$_3$), 2.01 (1H, s, OH) ppm. ^{13}C NMR (100 MHz, CDCl$_3$, 298 K): δ_C 211.92 (s, C≡O), 139.73−128.85 (m, Ph-C), 66.14 (s, C-O), 44.18−42.99 (m, SC), 21.06−20.86 (m, Ph-CH$_3$) ppm. Solution IR (CH$_2$Cl$_2$): νC≡O 2037 (s), 1997 (s) and 1958 (s) cm^{-1}.

[Re]-[NiFe$_2$]. 4-Dimethylaminopyridine (DMAP, 10 mg, 0.08 mmol) and *N*,*N*′-dicyclohexylcarbodiimide (DCC, 62 mg, 0.3 mmol) were added to a solution of [NiFe$_2$]−OH (67 mg, 0.1 mmol) and ReCl(CO)$_3$(CH$_3$-bpy-COOH) (115 mg, 0.22 mmol) in CH$_2$Cl$_2$ (40 mL) at 0 °C, and the reaction was stirred for 48 h at room temperature. The resulting suspension was filtered, and the filtrate was evaporated to dryness to yield the crude product, [Re]-[NiFe$_2$], which was purified by column chromatography on silica gel (Fluka, F60) using ethyl acetate and petroleum ether (bp 60−80 °C; 2/1, v/v) as eluent. The intensely colored slow-moving red/brown band was isolated, and removal of the solvent under reduced pressure afforded the target complex [Re]-[NiFe$_2$]. Yield 55 mg, 48%. Elemental Analysis: Found (Calculated for C$_{38}$H$_{26}$ClFe$_2$N$_2$NiO$_{11}$ReS$_4$) C, 37.78 (37.82); H, 2.19 (2.17); N, 2.36 (2.32)%. MS (ES$^-$) *m/z*: 1250.7685 [M + HCOO]$^-$, 1240.7342 [M + Cl]$^-$. The adduct [M + COOH]$^-$ shows an isotope pattern in good agreement with the theoretical value (Figure S1). ^{1}H NMR (300 MHz, CDCl$_3$, 298 K) δ: 2.39 (m, 9H, CH$_3$), 3.04 (m, 2H, SCH$_2$CHLCH$_2$S), 3.72 (m, 2H, SCH$_2$CHLCH$_2$S), 4.11 (m, 1H, SCH$_2$CHLCH$_2$S), 6.71−9.38 (m, 12H, Ph-H and Py-H) ppm. ^{13}C NMR (75 MHz, CDCl$_3$, 298 K) δ: 21.83 (m, CH$_3$), 33.96 (s, SCH$_2$CHLCH$_2$S), 49.19 (s, SCH$_2$CHLCH$_2$S), 118.78−156.05 (m, Ph-C and Py-C), 212.21 (s, CO) ppm. Solution IR: (CH$_2$Cl$_2$) ν(C≡O) 2037 (s), 2023 (s), 1997 (s), 1957 (s), 1920 (s) and 1900 (s) cm^{-1}, ν(C═O) 1737 (w) cm^{-1}; (CH$_3$CN) ν(C≡O) 2036 (s), 2023 (s), 1996 (s), 1957 (s), 1919 (s), 1901 (s) cm^{-1}, ν(C═O) 1742 (w) cm^{-1}.

Time-Resolved Infrared Spectroscopy. Picosecond and nanosecond TRIR spectra were obtained using purpose-built equipment based on a pump−probe approach at both Nottingham and the Rutherford Appleton Laboratory. Details of the equipment and methods used for the TRIR studies have been described previously.[19] The results were repeated on both instruments, but the data shown in this paper were obtained using the latter, which used a seeded dual titanium sapphire chirped pulse amplifier to generate 10 kHz, 40−80 fs, 0.8 mJ pulses at 800 nm. The beam was focused and split into 0.4 mJ beams, which were used to pump a number of different computer-controlled optical paramagnetic amplifiers (OPAs). These were able to output a range of synchronized wavelength combinations for use as either pump or probe beams with a 240 to 15 000 nm spectral coverage. A high-precision translation stage (Newport IMS600LM) provided a delay line for the pump beam and generates femtosecond to nanosecond pump−probe timing. Once through the sample the IR beam was collimated and focused onto a spectrograph where a 128 mercury cadmium telluride array detector was used to detect the mid-IR probe. Access to the nanosecond-to-microsecond time delays was provided by a nanosecond laser system, delivering 1064 nm pulses (10 kHz, 1 ns, 0.05 mJ). Pump energies of 1 μJ were typically used in experiments reported in this paper. The 355 nm harmonic was used, delivering >5 μJ energy per pulse, synchronized to the probe beam of the laser system described above. Samples were recirculated using a peristaltic pump as the sample was rastered in the *x* and *y* planes to minimize cumulative photodamage to both the sample and window during repeated photolysis. To analyze the reaction kinetics of transient species, the spectra were fitted using the minimum number of Lorentzian bands. In experiments containing [Re]/[NiFe$_2$], the intermediate growth and decay of the bands associated with [ReCl(CO)$_3$(CH$_3$-bpy-COOCH$_3$)]$^-$ overlap with either the parent bleaches of [NiFe$_2$] or the transient peaks of [NiFe$_2$]$^-$. As a result, the kinetics of [ReCl(CO)$_3$(CH$_3$-bpy-COOCH$_3$)]$^-$ was measured from the regrowth of the parent bands of [ReCl(CO)$_3$(CH$_3$-bpy-COOCH$_3$)], as multiple band fitting resulted in more tractable data analysis. For the same reason, the lifetime of [Re]$^-$-[NiFe$_2$] was measured from the regrowth of the parent bands of the [Re] moiety in [Re]-[NiFe$_2$].

Luminescence Spectroscopy. An Edinburgh Instruments FLS920 combined fluorescence lifetime and steady-state spectrometer was used for all emission measurements. Samples were held in a l × 1 cm quartz fluorescence cuvette and either degassed using three freeze−pump−thaw cycles on a Schlenk line or prepared in a glovebox. Excited-state lifetime measurements were performed using

DOI: 10.1021/acs.inorgchem.5b01744
Inorg. Chem. 2016, 55, 527−536

the time-correlated photon counting method, with a pulsed diode laser (EPL-405, Edinburgh Instruments) as an excitation source.

Electrochemical Measurements. Electrochemical measurements were made using an Autolab PGSTAT20 potentiostat. All solutions were purged with a stream of Ar prior to use. Cyclic voltammograms were performed using a three-electrode system, with a glassy carbon working electrode (6.7 mm diameter), a Pt wire secondary electrode, and a saturated calomel reference electrode. Before each measurement, the glassy carbon working electrode was cleaned using a polishing pad. All potentials are referenced to the Fc^+/Fc (Fc = ferrocene) couple, used as an internal standard. Cyclic voltammograms of [Re]-[$NiFe_2$] and [$NiFe_2$] (ca. 1 mM) in CH_2Cl_2 were recorded with $[NBu]_4[BF_4]$ (0.4 M) as a supporting electrolyte. Coulometric measurements were performed using an H-cell at 273 K in CH_2Cl_2 containing $[NBu_4][BF_4]$ (0.4 M); the cell consisted of a Pt/Rh gauze basket working electrode separated by a glass frit from a Pt/Rh gauze secondary electrode. The saturated calomel reference electrode was placed in a bridge tube containing electrolyte solution, the tip was positioned at the center of the working electrode, and the solution was stirred rapidly during electrolysis using a magnetic stirring bar. Catalytic cyclic voltammetry experiments were conducted using a sealed single-compartment electrochemical cell purged with Ar. Additions of TFA (0.1 mL, 0.5 M in CH_2Cl_2) to a solution of [Re]-[$NiFe_2$] or [$NiFe_2$] (5 mL, 1 mM in CH_2Cl_2) with $[NBu_4][BF_4]$ (0.4 M) were made using a gastight syringe (Hamilton TLL, Series 1700, model 1702 and 1705). UV−vis spectro-electrochemical experiments were performed either at 273 or 243 K with an optically transparent electrode inserted into a modified quartz cuvette with a path length of 0.5 mm. A three-electrode configuration consisting of a Pt/Rh gauze working electrode, a Pt wire secondary electrode (in a fritted poly(tetrafluoroethylene) sleeve), and a saturated calomel electrode (chemically isolated from the test solution via a bridge tube containing electrolyte solution and terminated in a porous frit) was used in the cell. The potential at the working electrode was controlled by a Sycopel Scientific Ltd. DD10 M potentiostat. The UV−vis spectra were recorded on a PerkinElmer Lambda 16 spectrophotometer at 1 nm resolution. The spectrometer cavity was purged with N_2, and temperature control at the sample was achieved by flowing cooled N_2 across the surface of the cell. FTIR and EPR spectroscopic measurements were run on aliquots of solutions following electrochemical bulk reduction.

H_2 Production. H_2 production experiments were conducted on purpose-built apparatus, the details of which have been reported previously.[12a] Irradiation was performed using a Xe arc lamp (Oriel Instruments, λ < 420 nm cutoff filter) operating at 250 W and H_2 was detected on a gas chromatograph (Shimadzu 2014) using a thermal conductivity detector operating at 50 °C.

RESULTS AND DISCUSSION

Electrochemical Studies. *Cyclic Voltammetry.* The cyclic voltammograms of [Re]-[$NiFe_2$] (1 mM) in CH_2Cl_2 (Figure 2) show two reduction processes at $E_{1/2}$ = −1.23 V and $E_{1/2}$ = −1.55 V versus Fc^+/Fc. The process at $E_{1/2}$ = −1.23 V versus Fc^+/Fc is an electrochemically reversible one-electron process and may be assigned to the reduction of the [$NiFe_2$] unit in [Re]-[$NiFe_2$] by comparison with the reduction process of [$NiFe_2$] ($E_{1/2}$ = −1.31 V vs Fc^+/Fc).[14] The second process at $E_{1/2}$ = −1.55 V versus Fc^+/Fc occurs at a comparable potential to $[ReCl(CO)_3(bpy)]$ and similar functionalized bipyridine compounds, and it is assigned to the reduction of the diimine ligand within the [Re] unit.[15,20] Coulometric studies show that this reduction process exhibits multielectron behavior, which may result from the instability of the diimine radical under the conditions of the experiment.[21] The cyclic voltammogram of [Re]-[$NiFe_2$] at 100 mV s^{-1} shows additional reduction processes at potentials more negative than −1.9 V versus Fc^+/Fc (Figure S2). These reductions and their associated

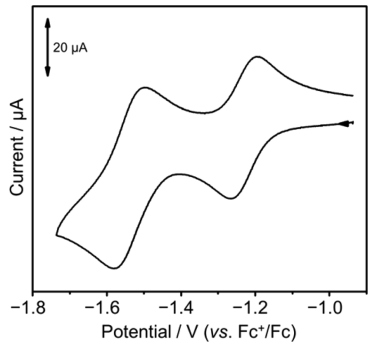

Figure 2. Cyclic voltammogram of [Re]-[$NiFe_2$] (1 mM) in CH_2Cl_2 containing $[NBu_4][BF_4]$ (0.4 M) as a supporting electrolyte showing the two reduction processes at $E_{1/2}$ = −1.23 V and $E_{1/2}$ = −1.55 V vs Fc^+/Fc.

oxidation waves were not studied further. The reduction processes of [Re]-[$NiFe_2$] at $E_{1/2}$ = −1.23 V and $E_{1/2}$ = −1.55 V versus Fc^+/Fc were investigated further with UV−vis, FTIR, and EPR spectroscopic methods.

UV−vis Spectroelectrochemical Studies. The one-electron reduction process at $E_{1/2}$ = −1.23 V versus Fc^+/Fc of [Re]-[$NiFe_2$] (1 mM) in CH_2Cl_2 was monitored by UV−vis spectroelectrochemistry at 243 K. During the reduction the intensity of the peaks at 372, 485, and 700 nm decrease with the simultaneous growth of new absorbances at 364, 420, 497, and 620 nm (Figure 3a and Table S1). These new bands are assigned to the reduction of the [$NiFe_2$] center to form [Re]-[$NiFe_2$]$^-$ through comparison with previously reported

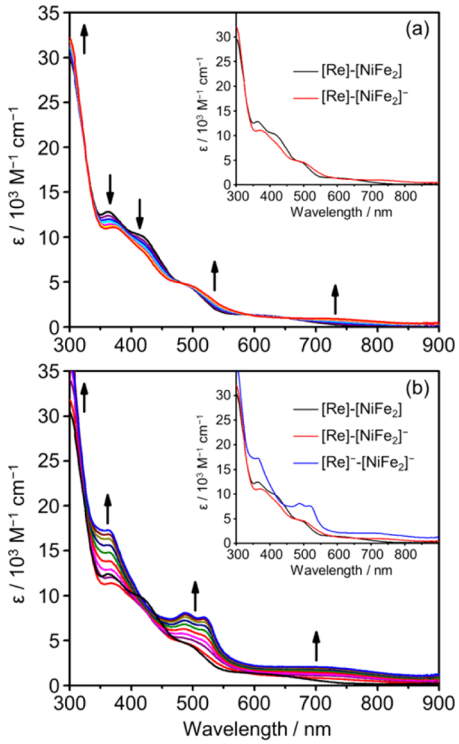

Figure 3. UV−vis spectra observed during the electrochemical reduction of [Re]-[$NiFe_2$] (1 mM) in CH_2Cl_2 (containing 0.4 M $[NBu_4][BF_4]$ as a supporting electrolyte) at 243 K. (a) Reduction of [Re]-[$NiFe_2$] (black) to [Re]-[$NiFe_2$]$^-$ (red). (b) Reduction of [Re]-[$NiFe_2$] (black) to [Re]$^-$-[$NiFe_2$]$^-$ (blue).

DOI: 10.1021/acs.inorgchem.5b01744
Inorg. Chem. 2016, 55, 527−536

spectroelectrochemical studies on [$NiFe_2$].[14] The presence of isosbestic points (Figure 3a and Table S1) are diagnostic of a conversion between [Re]-[$NiFe_2$] and [Re]-[$NiFe_2$]$^-$ occurring with no long-lived intermediates on the time scale of the experiment. Reoxidation of [Re]-[$NiFe_2$]$^-$ resulted in the quantitative regeneration of the UV−vis spectrum of [Re]-[$NiFe_2$], and thus, the reduction process is chemically reversible on the time scale of the experiment. The second reduction process at $E_{1/2}$ = −1.55 V versus Fc^+/Fc (Figure 2) was investigated by in situ bulk reduction of [Re]-[$NiFe_2$] at −1.65 V versus Fc^+/Fc (243 K, Figure 3b). This reduction process is associated with the development of bands at 374, 488, 520, and 699 nm (Figure 3b, Table S1), and these bands are assigned to reduction processes that are localized on both the bipyridine ligand of the [Re] unit and the [$NiFe_2$] moiety to generate [Re]$^-$-[$NiFe_2$]$^-$. Electrochemical oxidation of this solution generated an almost identical profile to [Re]-[$NiFe_2$] but with a decreased spectral intensity at ca. 370 nm. This difference is most likely due to the instability of the reduced bipyridine radical about the [Re] center observed previously in the coulometric experiments (see above).

FTIR and EPR Spectroscopic Studies. The FTIR spectrum of [Re]-[$NiFe_2$] (1 mM) in CH_2Cl_2 shows six distinct peaks (Figure 4) in the metal carbonyl region, which can be assigned

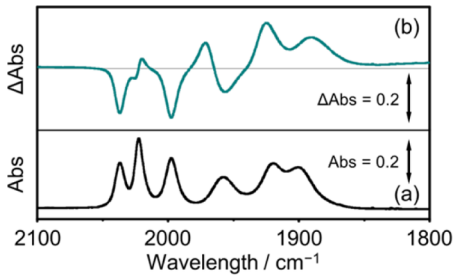

Figure 4. FTIR spectra of [Re]-[$NiFe_2$] before and after bulk reduction to [Re]-[$NiFe_2$]$^-$ in CH_2Cl_2 (containing 0.4 M [NBu_4]-[BF_4] as a supporting electrolyte) at 293 K. (a) FTIR spectrum of [Re]-[$NiFe_2$]. (b) FTIR difference spectrum recorded following the reduction of [Re]-[$NiFe_2$] to [Re]-[$NiFe_2$]$^-$.

to the [Re] (2023, 1920, and 1900 cm^{-1}) and [$NiFe_2$] (2037, 1997, and 1957 cm^{-1}) units. One electron reduction at −1.23 V versus Fc^+/Fc is associated with a decrease in intensity of bands at 2037, 1997, and 1957 cm^{-1} and the growth of new bands at 1972, 1925, and 1890 cm^{-1} (Figure 4, green line), which are associated with a one-electron reduced [$NiFe_2$] unit. The down shift of ca. 67 cm^{-1} for the CO bands in [Re]-[$NiFe_2$]$^-$ relative to those in [Re]-[$NiFe_2$] is in good agreement with shifts reported for other [$NiFe_2$] centers and is indicative of an increased electron density on the Fe centers.[10a,12] A small reduction in the intensity of a band associated with the [Re] unit (2025 cm^{-1}) can also be observed in the spectrum along with the growth of a band at 2020 cm^{-1}. It appears that during bulk electrolysis partial reaction at the [Re] center occurs. X-band EPR spectra of electrochemically generated [Re]-[$NiFe_2$]$^-$ were recorded as fluid (293 K) and frozen (77 K) solutions (Figure 5). The simulated Hamiltonian parameters (g_{iso} = 2.043; g_{11} = 2.014; g_{22} = 2.018; and g_{33} = 2.098) are in good agreement with the those reported for [$NiFe_2$]$^-$ (g_{iso} = 2.042; g_{11} = 2.099; g_{22} = 2.015; and g_{33} = 2.015).[14]

Electrocatalytic Studies. The electrocatalytic activity of the first reduction process of [Re]-[$NiFe_2$] ($E_{1/2}$ = −1.23 V vs Fc^+/Fc) was investigated using the same procedure that has been employed previously for [$NiFe_2$] and related compounds.[12b,14] The cyclic voltammogram of [Re]-[$NiFe_2$] shows an increased cathodic peak current and a reduction in the current of the anodic wave (Figure S3), as aliquots of TFA are added to a solution of [Re]-[$NiFe_2$] (1 mM) in CH_2Cl_2 (containing 0.4 M [NBu_4][BF_4] as a supporting electrolyte). This reduction in the current of the anodic wave is consistent with the removal of [Re]-[$NiFe_2$]$^-$ from the diffusion layer of the working electrode by a method other than that of heterogeneous electron transfer to the electrode and is diagnostic of an electrocatalytic process.[22]

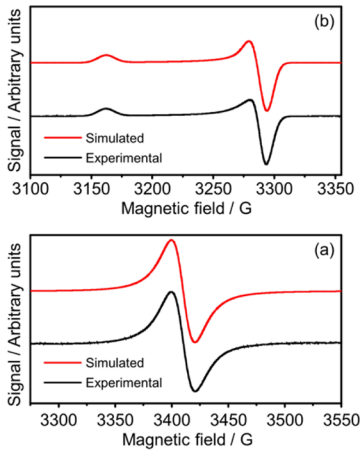

Figure 5. X-band EPR spectra in CH_2Cl_2 (black) and the simulated spectra (red) for [Re]-[$NiFe_2$]$^-$ (a) as a fluid solution at 293 K (simulation parameters: g_{iso} = 2.043; W_{iso} = 20 G) and (b) as a frozen solution at 77 K (simulation parameters: g_{11} = 2.014; g_{22} = 2.018; g_{33} = 2.098; W_{11} = 11 G; W_{22} = 12 G; W_{33} = 14 G).

The electrochemical and spectrochemical results are consistent with a first reduction process that is localized at the [$NiFe_2$] center and a second process that is localized at the [Re] center in [Re]-[$NiFe_2$]. Thus, the photoreduction of the [Re] unit could provide a route to the photochemical production of [Re]-[$NiFe_2$]$^-$, a desired intermediate required for catalytic H_2 formation.

Luminescence Spectroscopic Studies. The excited-state properties of the linked dyad [Re]-[$NiFe_2$] and of the analogous uncoupled [Re]/[$NiFe_2$] system were examined by luminescence spectroscopy. Luminescence spectra of solutions containing [Re]-[$NiFe_2$], [$ReCl(CO)_3(CH_3$-bpy-$COOCH_3)$], [$NiFe_2$], and [Re]/[$NiFe_2$] (each at 17 μM) in CH_3CN are shown in Figure 6 (λ_{ex} = 406 nm).

The observed emission for each solution (except [$NiFe_2$]) was normalized to the absorbance at 406 nm in the UV−vis spectrum. For solutions of [Re]/[$NiFe_2$] and [Re]-[$NiFe_2$] the spectral bands of [$NiFe_2$] were subtracted before normalization. [$ReCl(CO)_3(CH_3$-bpy-$COOCH_3)$] exhibits a broad emission (λ_{max} = 678 nm, τ = 25 ± 0.5 ns, Figure 6, green line), and the addition of an equimolar amount of [$NiFe_2$] to the solution resulted in no observable drop in the emission intensity or lifetime of the ^{3}MLCT excited state ([Re]/[$NiFe_2$], Figure 6, black line). This suggests that at concentrations of ca. 17 μM, [$NiFe_2$] does not quench the ^{3}MLCT excited state of [$ReCl(CO)_3(CH_3$-bpy-$COOCH_3)$] to a detectable extent. In contrast, the emission from [Re]-[$NiFe_2$] is ca. 60% lower in intensity (λ_{max} = 650 nm, τ = 24 ± 0.5 ns, Figure 6, red line) when compared to [Re]/[$NiFe_2$]. The drop in emission

DOI: 10.1021/acs.inorgchem.5b01744
Inorg. Chem. 2016, 55, 527−536

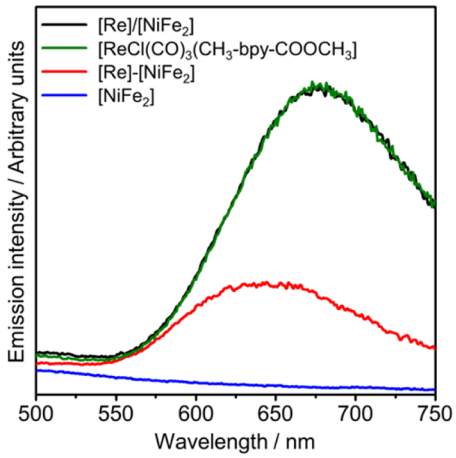

Figure 6. Luminescence spectra for [Re]/[$NiFe_2$], [$ReCl(CO)_3(CH_3$-bpy-$COOCH_3$)], [Re]-[$NiFe_2$], and [$NiFe_2$] (each at 17 μM) in CH_3CN (λ_{ex} = 406 nm).

intensity could suggest quenching of the [Re]-based excited state in [Re]-[$NiFe_2$] by the covalently bound [$NiFe_2$] moiety. However, the lifetimes are not significantly different, and the emission maximum for [Re]-[$NiFe_2$] is at a higher energy than for [$ReCl(CO)_3(CH_3$-bpy-$COOCH_3$)].

We estimated the quenching rate constant (k_q) for the reductive quenching of the ^{3}MLCT excited states of [Re]-[$NiFe_2$] and [$ReCl(CO)_3(CH_3$-bpy-$COOCH_3$)] by NEt_3, through construction of Stern−Volmer plots generated from the ^{3}MLCT lifetime (Figure S4).[23] The second-order quenching rate constants are k_q = 4.3 ± 0.2 × 10^7 M^{-1} s^{-1} (Figure S4, black dots) and k_q = 1.4 ± 0.1 × 10^7 M^{-1} s^{-1} (Figure S4, black squares) for the ^{3}MLCT excited state of [$ReCl(CO)_3(CH_3$-bpy-$COOCH_3$)] and [Re]-[$NiFe_2$], respectively.

Time-Resolved Infrared Spectroscopic Studies. We used picosecond- and nanosecond-TRIR spectroscopies to probe the mechanisms of the decay of the excited states in [Re]-[$NiFe_2$] and [Re]/[$NiFe_2$] in CH_3CN, where the reaction kinetics can be elucidated and used to monitor electron transfer processes.

Time-Resolved Infrared Studies on [Re]-[$NiFe_2$]. The FTIR spectrum of [Re]-[$NiFe_2$] in CH_3CN possesses six ν(CO) bands associated with the [Re] (2023, 1919, and 1901 cm^{-1}) and [$NiFe_2$] (2036, 1996, and 1957 cm^{-1}) units of the molecule (Figure 7a). The picosecond-TRIR spectrum of [Re]-[$NiFe_2$] (0.3 mM) obtained 50 ps after flash photolysis (λ = 400 nm) shows that all parent bands are bleached and that new bands are observed at 2065, 2009, 1985, and 1945 cm^{-1} (Figure 7b). The transient species in this spectrum can be divided into two components, those associated with the [Re] and those with the [$NiFe_2$] units. The parent bands associated with the [$NiFe_2$] center rapidly reform (τ = 70 ps, Figure S5) as the bands at 2009 and 1985 cm^{-1} decay, which is similar to processes observed in the control experiment following the photolysis of [$NiFe_2$], in which a short-lived transient is formed (τ = 90 ps) with bands shifted to lower wavenumber.[12a] This species is tentatively assigned to the homolysis of the Fe−Fe bond in [$NiFe_2$], which has also been observed after photolysis of synthetic analogues of the active sites of the [FeFe] hydrogenases.[5d,9a] The nanosecond-TRIR spectrum of [Re]-[$NiFe_2$] recorded 2 ns after photolysis (λ = 355 nm) only shows depletion of the parent bands associated with the [Re]

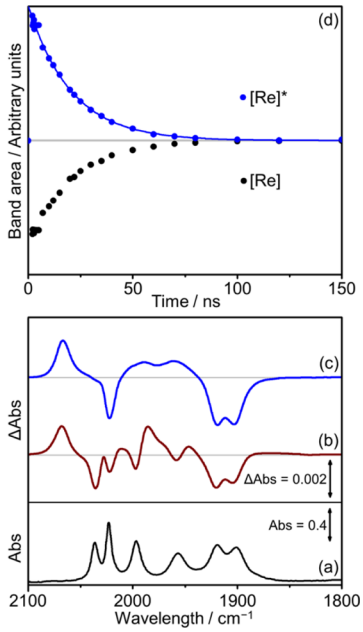

Figure 7. FTIR, ps-TRIR, and ns-TRIR spectra of [Re]-[$NiFe_2$] in CH_3CN. (a) FTIR ground-state spectrum. (b) ps-TRIR difference spectrum taken 50 ps after flash photolysis at 400 nm. (c) ns-TRIR difference spectrum taken 2 ns after flash photolysis at 355 nm. (d) TRIR kinetic traces for the decay of the [Re]* center (blue dots) and regrowth of the ground-state bands, [Re] (black dots). The solid blue line is a monoexponential best-fit of the data.

moiety (2023, 1919, and 1901 cm^{-1}) and transient bands at 2065, 1995, and 1960 cm^{-1} (Figure 7c, blue line). The species formed is characteristic of the production of a Re-diimine ^{3}MLCT excited state where the ν(CO) bands shift up in energy due to the oxidation of the Re center ([Re]*-[$NiFe_2$]).[24] Such behavior has been reported for numerous [$ReCl(CO)_3$(diimine)] ^{3}MLCT excited states, and the shift in the ν(CO) bands to higher wavenumber has been well-documented.[25] Following photolysis, the ^{3}MLCT bands decay (τ = 20 ± 1 ns, Figure 7d, blue dots), and the parent bands reform (Figure 7d, black dots). This lifetime (τ = 20 ± 1 ns) is of the same magnitude as the ^{3}MLCT emission lifetime at 650 nm (τ = 24 ± 0.5 ns), measured using luminescence spectroscopy (see above) and suggests that the excited state [Re]*-[$NiFe_2$] is not quenched by electron transfer to the [$NiFe_2$] unit.

Figure 8 shows the nanosecond-TRIR spectra obtained following excitation (λ = 355 nm) of [Re]-[$NiFe_2$] (0.3 mM) in a solution of CH_3CN containing NEt_3 (2 M). The spectrum obtained 2 ns after photolysis (Figure 8b) is identical to the spectra obtained above in the absence of NEt_3 (Figure 7c) and shows the formation of a ^{3}MLCT excited state at the [Re] center. However, in this experiment the ^{3}MLCT bands decay (Figure 8e, blue dots, τ = 12 ± 0.5 ns) as 60% of the parent [Re] moiety bands recover (Figure 8e, black dots) to form a new species with bands at 2004, 1896, and 1897 cm^{-1} (Figure 8c), which accounts for the remaining 40% of the parent bleach. Through comparison with similar experiments on Re-diimine complexes,[26] this new species can be assigned as [$Re]^-$-[$NiFe_2$] formed through reductive quenching of [Re]*-[$NiFe_2$] by NEt_3. On a longer time scale (100−10 000 ns) [$Re]^-$-[$NiFe_2$] decays (τ = 3100 ± 100 ns, Figure 8e, red dots), and the remaining bands associated with the [Re] center recover.

DOI: 10.1021/acs.inorgchem.5b01744
Inorg. Chem. 2016, 55, 527−536

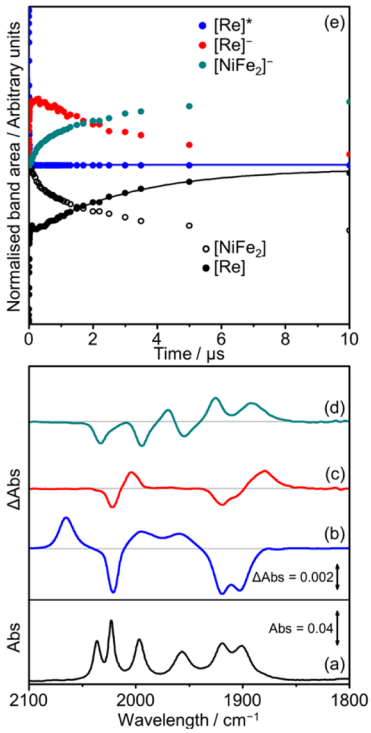

Figure 8. FTIR and nanosecond-TRIR spectra of [Re]-[$NiFe_2$] in a solution of CH_3CN containing NEt_3 (2 M). (a) FTIR ground state spectrum. nanosecond-TRIR difference spectra taken (b) 2 ns, (c) 50 ns, and (d) 50 μs after flash photolysis at 355 nm. (e) TRIR kinetic traces for the decay of the ^{3}MLCT excited state, [Re]*-[$NiFe_2$] (blue); the growth and decay of [$Re]^-$-[$NiFe_2$] (red dots), the growth of [Re]-[$NiFe_2]^-$ (green), the regeneration of the [Re] center (black ●), and the loss of the [$NiFe_2$] center (black ○). The solid black line is a monoexponential best fit of the data.

Concomitantly the ν(CO) bands of the [$NiFe_2$] unit are bleached (Figure 8e, black circles), and bands associated with the formation of [Re]-[$NiFe_2]^-$ grow in at 1970, 1926, and 1889 cm^{-1} (Figure 8d). Thus, electron transfer involving [$Re]^-$-[$NiFe_2$] occurs to form [Re]-[$NiFe_2]^-$ via a reductive quenching pathway from the ^{3}MLCT of the photosensitizing unit. The growth of [Re]-[$NiFe_2]^-$ (100−10 000 ns) is biexponential (Figure 8e, green dots); a possible consequence of its formation from [$Re]^-$-[$NiFe_2$] and from the decomposition of the oxidized electron donor ($^{\bullet}NEt_3^+$). This process has been observed previously for similar Re-diimine complexes following reductive quenching by NEt_3 or TEOA.[12a,27] We have also observed similar behavior in photolysis experiments involving [$ReCl(CO)_3$(bpy)] and [$NiFe_2$] in a solution of CH_3CN containing NEt_3.[12a] In this example decomposition of NEt_3 resulted in the reduction of [$NiFe_2$] to [$NiFe_2]^-$. Once formed, [Re]-[$NiFe_2]^-$ remains stable on the time scale of this experiment (up to 70 μs).

Time-Resolved Infrared Studies on [Re]/[$NiFe_2$]. A previous picosecond-TRIR investigation of [$NiFe_2$] in CH_3CN has shown that a short-lived transient (τ = 90 ps) is formed following photolysis with characteristic bands shifted to lower wavenumber, namely, [$NiFe_2$]* (see above). The presence of NEt_3 did not affect the lifetime or band positions of [$NiFe_2$]*, and no direct interaction between [$NiFe_2$]*, [$ReCl(CO)_3$(bpy)], or the ^{3}MLCT excited state of [$ReCl(CO)_3$(bpy)] was observed on these time scales.[12a] Therefore, to simplify the analysis of the spectra in this study, solutions containing [$NiFe_2$] at time delays of less than 2 ns after excitation are not reported.

Figure S6a shows the ground-state FTIR spectrum of [Re]/[$NiFe_2$] with three bands associated with [$ReCl(CO)_3(CH_3$-bpy-$COOCH_3)$] (2023, 1919, and 1901 cm^{-1}) and three with [$NiFe_2$] (2035, 1995, and 1955 cm^{-1}). The nanosecond-TRIR spectrum recorded 2 ns after the photolysis of a solution of [Re]/[$NiFe_2$] (both at 1 mM) in CH_3CN is shown in Figure S6b. Depletion of the parent [$ReCl(CO)_3(CH_3$-bpy-$COOCH_3)$] bands are observed with the formation of a species at 2067, 1997, and 1959 cm^{-1} characteristic of the production of a Re-diimine ^{3}MLCT excited state ([$ReCl(CO)_3(CH_3$-bpy-$COOCH_3)$]*). [$ReCl(CO)_3(CH_3$-bpy-$COOCH_3)$]* decays back to the ground state (τ = 22 ± 1 ns) as the parent bleaches for [$ReCl(CO)_3(CH_3$-bpy-$COOCH_3)$] recover and the rate of decay is similar to the ^{3}MLCT emission (τ = 25 ± 0.5 ns) measured above using luminescence spectroscopy. The CO bands corresponding to [$NiFe_2]^-$ were not observed, which suggests that electron transfer from [$ReCl(CO)_3(CH_3$-bpy-$COOCH_3)$]* to [$NiFe_2$] does not occur to an extent that can be monitored in these experiments.

Figure S7 shows the nanosecond-TRIR spectra recorded following photolysis (λ = 355 nm) of [$ReCl(CO)_3(CH_3$-bpy-$COOCH_3)$] (0.5 mM) in a solution of CH_3CN containing NEt_3 (1 M). Bands characteristic of [$ReCl(CO)_3(CH_3$-bpy-$COOCH_3)$]* are observed to form 4 ns after excitation (Figure S7b). [$ReCl(CO)_3(CH_3$-bpy-$COOCH_3)$]* (τ = 10 ± 2 ns) is reductively quenched by NEt_3 to form [$ReCl(CO)_3(CH_3$-bpy-$COOCH_3)]^-$ (43%) with bands at 2000, 1891, and 1894 cm^{-1}, while the remaining 57% decays back to the ground state. The rise in [$ReCl(CO)_3(CH_3$-bpy-$COOCH_3)]^-$ is observed as two processes over two different time scales (Figure S7d, red dots). The first phase (0−70 ns), which occurs on a similar time scale to the decay of the ^{3}MLCT excited stated, is associated with the reductive quenching process described above involving [$ReCl(CO)_3(CH_3$-bpy-$COOCH_3)$] and NEt_3. The second phase (70−1000 ns) can be explained by considering the decomposition of the oxidized electron donor $^{\bullet}NEt_3^+$, which may result in the reduction of a second equivalent of [$ReCl(CO)_3(CH_3$-bpy-$COOCH_3)$] as was observed previously for the reduction of [Re]-[$NiFe_2$].

[Re]/[$NiFe_2$] (1 mM) was investigated in a solution of CH_3CN containing NEt_3 (2 M). [$ReCl(CO)_3(CH_3$-bpy-$COOCH_3)$]* is observable 2 ns after photolysis as a transient in the spectrum (Figure S8b). This ^{3}MLCT excited state decays (τ = 10 ± 2 ns, Figure S8e, blue dots) to the ground state (57%) and through reductive quenching by NEt_3 (43%) to form [$ReCl(CO)_3(CH_3$-bpy-$COOCH_3)]^-$ (Figure S8c). Over greater time scales (50−1500 ns), the CO bands associated with [$ReCl(CO)_3(CH_3$-bpy-$COOCH_3)]^-$ are lost (τ = 250 ± 10 ns, Figure S8e, red dots) as this species reduces [$NiFe_2$] to [$NiFe_2]^-$ to generate a spectrum with bands at 1969, 1921, and 1896 cm^{-1} (Figure S8d). [$NiFe_2]^-$ remains stable for the time scale of the experiment (70 μs).

The most noticeable difference in the excited-state electron transfer mechanisms in [Re]-[$NiFe_2$] and [Re]/[$NiFe_2$] is the lifetime of the reduced photosensitizer. The monoexponential decay of [$ReCl(CO)_3(CH_3$-bpy-$COOCH_3)]^-$ (τ = 250 ± 10 ns, Figure S8e, red dots) is significantly shorter than that measured for [$Re]^-$-[$NiFe_2$] (τ = 3100 ± 100 ns, Figure 8e, red dots) under similar conditions. This faster rate for [Re]/[$NiFe_2$] was investigated further by the determination of the

DOI: 10.1021/acs.inorgchem.5b01744
Inorg. Chem. 2016, 55, 527−536

rate constants of the electron transfer processes in both [Re]-[$NiFe_2$] and [Re]/[$NiFe_2$].

Concentration-Dependent Time-Resolved Infrared Studies. Nanosecond-TRIR experiments have shown that the reduction of the [$NiFe_2$] center in [Re]-[$NiFe_2$] can be achieved via the photochemical formation of $[Re]^-$-[$NiFe_2$] and subsequent electron transfer to generate [Re]-$[NiFe_2]^-$. We performed concentration-dependent studies to determine the mechanism of this electron transfer process in [Re]-[$NiFe_2$] and [Re]/[$NiFe_2$]. For [Re]/[$NiFe_2$] only intermolecular electron transfer is possible (eq 1) with the observed rate constant expected to exhibit pseudo-first-order kinetics and to be dependent on [$NiFe_2$] concentration. However, in the case of [Re]-[$NiFe_2$], both intra- and intermolecular electron transfer processes are feasible (eqs 2 and 3). Therefore, concentration-dependent analysis of the observed rate constant for electron transfer should be able to distinguish between the two mechanisms. The observed rate constant can be calculated from the reciprocal of the lifetime of either $[Re]^-$-[$NiFe_2$] or $[ReCl(CO)_3(CH_3\text{-bpy-}COOCH_3)]^-$.

$$[Re]^-/[NiFe_2] \xrightarrow{k_{inter}} [Re]/[NiFe_2]^- \quad (1)$$

$$[Re]^-\text{–}[NiFe_2] \xrightarrow{k_{intra}} [Re]\text{–}[NiFe_2]^- \quad (2)$$

$$[Re]^-\text{–}[NiFe_2] + [Re]\text{–}[NiFe_2] \xrightarrow{k_{inter}} [Re]\text{–}[NiFe_2] + [Re]\text{–}[NiFe_2]^- \quad (3)$$

To quantify the rate of electron transfer in [Re]/[$NiFe_2$] the concentrations of all components were kept constant (0.5 mM $[ReCl(CO)_3(CH_3\text{-bpy-}COOCH_3)]$; 1 or 2 M NEt_3) except for the concentration of [$NiFe_2$], which was varied between 0.34 and 1.00 mM. The lifetime dependence of $[ReCl(CO)_3(CH_3\text{-bpy-}COOCH_3)]^-$ on the concentration of [$NiFe_2$] is shown in Table S2 with the pseudo-first-order rate plot in Figure 9a. Since [$NiFe_2$] is in excess, its concentration remains almost constant, and so the observed pseudo-first-order rate constant can be used to calculate the second-order rate constant for electron transfer, $k_{inter} = 3.8 \pm 0.5 \times 10^9\ M^{-1}\ s^{-1}$. This is in a similar range to the value reported for electron transfer between $[ReCl(CO)_3(bpy)]^-$ and [$NiFe_2$], $k_{inter} = 6.7 \times 10^9\ M^{-1}\ s^{-1}$.[12a]

In a similar experiment, the concentration of [Re]-[$NiFe_2$] was varied between 0 and 0.3 mM (Figure 9b and Table S2). This concentration range was selected to reduce the overall absorbance at the excitation wavelength (355 nm). A similar trend to that for [Re]/[$NiFe_2$] is observed: as the concentration of [Re]-[$NiFe_2$] is increased the observed electron transfer rate constant also increases. However, it is not directly proportional to the concentration of [Re]-[$NiFe_2$] and does not pass close to the origin (Figure 9b). This could suggest that intra- *and* intermolecular pathways operate in this system. Thus, assuming that these two processes are the only significant processes occurring following photolysis, then the gradient of the linear fit provides an estimate of the intermolecular electron transfer rate constant, $k_{inter} = 5.9 \pm 0.7 \times 10^8\ M^{-1}\ s^{-1}$. The positive intercept of this line at 0 M [Re]-[$NiFe_2$] (Figure 9b) suggests that intramolecular electron transfer also occurs, the first-order rate constant of which can be estimated at $k_{intra} = 1.5 \pm 0.1 \times 10^5\ s^{-1}$. It must be noted that this simplification of the electron transfer mechanism does not include any potential effects resulting from the decomposition of the electron donor, NEt_3.

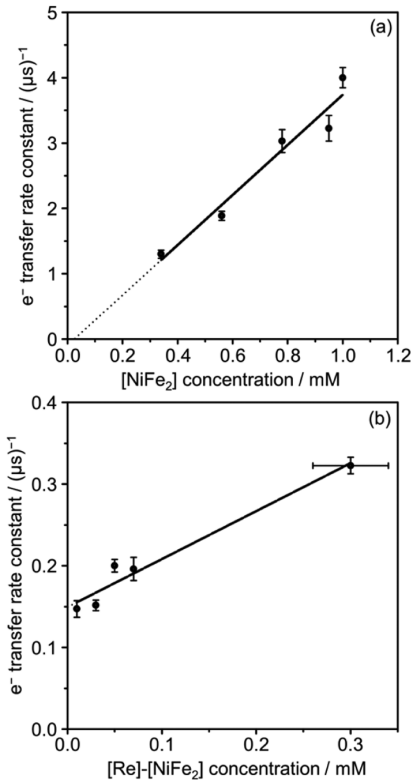

Figure 9. Variation of the observed electron transfer rate constants with catalyst concentration. (a) [Re]/[$NiFe_2$] in a solution of CH_3CN containing NEt_3, linear fitting (solid line) gives $k_{inter} = 3.8 \pm 0.5 \times 10^9\ M^{-1}\ s^{-1}$ (gradient). (b) [Re]-[$NiFe_2$] in a solution of NEt_3 and CH_3CN, linear fitting (solid line) gives $k_{inter} = 5.9 \pm 0.7 \times 10^8\ M^{-1}\ s^{-1}$ (gradient) and $k_{intra} = 1.5 \pm 0.1 \times 10^5\ s^{-1}$ (x = 0 intercept). Dashed lines are extensions of the linear fits.

Fourier Transform Infrared Steady-State Photochemical Studies. To assess the stability of [Re]-[$NiFe_2$] and [Re]/[$NiFe_2$] during continued photolysis, the FTIR spectrum was monitored following irradiation using white light from a light-emitting diode (LED; λ < 420 nm cutoff filter). Figure 10b shows the FTIR spectrum taken ca. 5 s after 1 min of photolysis of [Re]-[$NiFe_2$], and the bands originating from [Re]-$[NiFe_2]^-$ (1970, 1926, and 1889 cm^{-1}) are observed with an associated loss in the bands from the [$NiFe_2$] unit. In addition, bands at 1938 and 1909 cm^{-1} develop, and by comparison with our previous studies on [$NiFe_2$] in CH_3CN,[12a] these can be assigned as originating from the formation of a second isomer

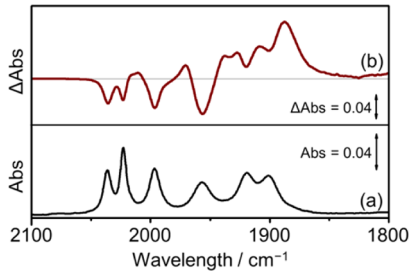

Figure 10. FTIR spectra of [Re]-[$NiFe_2$] before and after steady-state photolysis in a solution of CH_3CN containing NEt_3 (1 M). (a) Ground-state FTIR spectrum. (b) FTIR difference spectrum taken ca. 5 s after 1 min photolysis. In situ photolysis was performed using an LED white light source and a λ < 420 nm cutoff filter.

DOI: 10.1021/acs.inorgchem.5b01744
Inorg. Chem. 2016, 55, 527–536

of [Re]-[$NiFe_2$]$^-$, where the two of the terminal carbonyl bands of the [$NiFe_2$] unit bridge across the two Fe atoms. Depletion of the parent bands of the [Re] center is also evident and a broad positive feature is observed at 2013 cm^{-1}, which is in a similar region to related products reported following chemical reduction of [$ReCl(CO)_3(bpy)$]. These include [$ReCl(CO)_3(bpy)$]$^-$ (1998, 1880, and 1866 cm^{-1}, in CH_3CN), [$Re(CH_3CN)(CO)_3(bpy)$]$^\bullet$ (2017 and 1902(br) cm^{-1}, in CH_3CN), and [$Re(CO)_3(bpy)$]$_2$ (1990, 1952, 1886, and 1863 cm^{-1} in tetrahydrofuran);[28] however, the precise origin of the band in our experiment could not be determined. The apparent loss of bands associated with the [Re] center upon photolysis, without the clear formation of a new species, suggests that decomposition of the [Re] diimine center has occurred to yield products that are not clearly observable in this region of the IR spectrum.

A similar spectral profile was observed for [Re]/[$NiFe_2$] after 1 min of photolysis. Almost complete depletion of the bands originating from both [$ReCl(CO)_3(CH_3$-bpy-$COOCH_3)$] and [$NiFe_2$] can been seen with the formation of both isomers of [$NiFe_2$]$^-$ (Figure S9). This apparent decomposition of the photosensitizer in [Re]/[$NiFe_2$] was not observed when [$ReCl(CO)_3(bpy)$] was used in place of [$ReCl(CO)_3(CH_3$-bpy-$COOCH_3)$].[12a] In this example no apparent loss in the bands of [$ReCl(CO)_3(bpy)$] could be observed after 30 s of photolysis under similar conditions. Thus, it appears that functionalizing the bipyridine ligand in [Re]-[$NiFe_2$] and [$ReCl(CO)_3(CH_3$-bpy-$COOCH_3)$] reduces the stability of the photosensitizer when compared to [$ReCl(CO)_3(bpy)$], on continuous photolysis in reducing conditions.

H_2 Production Studies. We investigated the use of [Re]-[$NiFe_2$] and [Re]/[$NiFe_2$] for photoinduced H_2 production using both NEt_3 and TEOA as sacrificial electron donors. [$ReCl(CO)_3(bpy)$] has been used previously as a photosensitizer for photocatalytic H_2 production from [$NiFe_2$] with a TON of 55 under optimal conditions.[12a] Using similar conditions, [Re]-[$NiFe_2$] (0.1 mM) was investigated in a solution of CH_3CN containing TEOA (1 M) and [HTEOA]-[BF_4] (0.1 M) as a proton source. Only a trace amount of H_2 could be detected from this system, with a TON of ca. 1 based on [Re]-[$NiFe_2$] as the catalytic moiety. Replacing TEOA with NEt_3 had a negative effect on the total amount of H_2 evolved. In a solution containing [Re]/[$NiFe_2$] (both at 0.1 mM), TEOA (1 M), and [HTEOA][BF_4] (0.1 M) in CH_3CN, again only a trace amount of H_2 was evolved. Thus, from FTIR and H_2 production studies it appears that when either [Re]-[$NiFe_2$] or [Re]/[$NiFe_2$] are used for H_2 production, rapid decomposition of the esterified photosensitizer occurs, resulting in an almost complete loss in catalytic activity toward H_2 production.

CONCLUSIONS

We have investigated a linked dyad, [Re]-[$NiFe_2$] (Figure 1), designed for photoinduced electron transfer and proton reduction. Following flash photolysis, picosecond-TRIR and nanosecond-TRIR spectroscopies have monitored the reduction of the [$NiFe_2$] catalytic moiety in [Re]-[$NiFe_2$] and probed the mechanisms of electron transfer. Excitation of the [Re] center results in the population of the ^{3}MLCT excited state, [Re]*-[$NiFe_2$]. Reductive quenching of [Re]*-[$NiFe_2$] by NEt_3 forms [Re]$^-$-[$NiFe_2$], which subsequently undergoes electron transfer to the [$NiFe_2$] center to form [Re]-[$NiFe_2$]$^-$. The mechanisms of this electron transfer step were probed by concentration-dependent studies and suggest that both intra- and intermolecular electron transfer processes are involved ($k_{inter} = 5.9 \pm 0.7 \times 10^8$ M^{-1} s^{-1}, $k_{intra} = 1.5 \pm 0.1 \times 10^5$ s^{-1}). As expected, in the analogous bimolecular system ([Re]/[$NiFe_2$]), only intermolecular electron transfer could be observed ($k_{inter} = 3.8 \pm 0.5 \times 10^9$ M^{-1} s^{-1}). One of the key advantages for directly linking the photosensitizer and catalyst is to increase the rate of electron transfer. However, in this study the overall observed rate of electron transfer is significantly slower in [Re]-[$NiFe_2$] than in [Re]/[$NiFe_2$]. During continuous photolysis, rapid decomposition of the photosensitizing unit in both [Re]-[$NiFe_2$] and [Re]/[$NiFe_2$] can be observed using FTIR spectroscopy. This may, in part, help to explain the poor activity of this dyad and the bimolecular system toward H_2 evolution in acidic media. In the ester-linked dyad probed in this study, linking the catalytic and photosensitizing moieties appears to be detrimental to both the electron transfer rate and the chemical stability of the system on continuous photolysis. However, careful consideration in the development of future systems can overcome these problems so that the benefits of linked dyads can be exploited.

ASSOCIATED CONTENT

Supporting Information

The Supporting Information is available free of charge on the ACS Publications website at DOI: 10.1021/acs.inorgchem.5b01744.

Isotope pattern and exact mass comparison, cyclic voltammograms, tabulated UV−vis absorbance maxima and isosbestic points, Stern−Volmer plots, FTIR and TRIR spectra, tabulated kinetics data. (PDF)

AUTHOR INFORMATION

Corresponding Authors

*E-mail: M.Schroder@manchester.ac.uk. (M.S.)
*E-mail: J.McMaster@nottingham.ac.uk. (J.M.)
*E-mail: Mike.George@nottingham.ac.uk. (M.W.G.)

Notes

The authors declare no competing financial interest.

ACKNOWLEDGMENTS

We thank the EPSRC and the Univ. of Nottingham for support. M.S. acknowledges receipt of an ERC Advanced Grant.

REFERENCES

(1) (a) Faunce, T.; Styring, S.; Wasielewski, M. R.; Brudvig, G. W.; Rutherford, A. W.; Messinger, J.; Lee, A. F.; Hill, C. L.; deGroot, H.; Fontecave, M.; MacFarlane, D. R.; Hankamer, B.; Nocera, D. G.; Tiede, D. M.; Dau, H.; Hillier, W.; Wang, L. Z.; Amal, R. *Energy Environ. Sci.* **2013**, *6*, 1074−76. (b) Cowan, A. J.; Durrant, J. R. *Chem. Soc. Rev.* **2013**, *42*, 2281−93.

(2) (a) Karkas, M. D.; Johnston, E. V.; Verho, O.; Åkermark, B. *Acc. Chem. Res.* **2014**, *47*, 100−11. (b) Eckenhoff, W. T.; Eisenberg, R. *Dalton Trans.* **2012**, *41*, 13004−21.

(3) (a) Windle, C. D.; Perutz, R. N. *Coord. Chem. Rev.* **2012**, *256*, 2562−70. (b) Izumi, Y. *Coord. Chem. Rev.* **2013**, *257*, 171−86. (c) Benson, E. E.; Kubiak, C. P.; Sathrum, A. J.; Smieja, J. M. *Chem. Soc. Rev.* **2009**, *38*, 89−99.

(4) Han, Z.; Qiu, F.; Eisenberg, R.; Holland, P. L.; Krauss, T. D. *Science* **2012**, *338*, 1321−24.

(5) (a) Hammarström, L. *Acc. Chem. Res.* **2015**, *48*, 840−50. (b) Song, L.-C.; Liu, X.-F.; Xie, Z.-J.; Luo, F.-X.; Song, H.-B. *Inorg. Chem.* **2011**, *50*, 11162−72. (c) Berardi, S.; Drouet, S.; Francas, L.; Gimbert-Surinach, C.; Guttentag, M.; Richmond, C.; Stoll, T.; Llobet,

DOI: 10.1021/acs.inorgchem.5b01744
Inorg. Chem. 2016, 55, 527−536

A. *Chem. Soc. Rev.* **2014**, *43*, 7501−19. (d) Lomont, J. P.; Harris, C. B. *Inorg. Chim. Acta* **2015**, *424*, 38−50.
(6) (a) Gloaguen, F.; Rauchfuss, T. B. *Chem. Soc. Rev.* **2009**, *38*, 100−08. (b) Simmons, T. R.; Berggren, G.; Bacchi, M.; Fontecave, M.; Artero, V. *Coord. Chem. Rev.* **2014**, *270*, 127−150. (c) Woolerton, T. W.; Sheard, S.; Chaudhary, Y. S.; Armstrong, F. A. *Energy Environ. Sci.* **2012**, *5*, 7470−90. (d) Tard, C.; Pickett, C. J. *Chem. Rev.* **2009**, *109*, 2245−74.
(7) (a) Frey, M. *ChemBioChem* **2002**, *3*, 153−60. (b) Dawson, J.; Ghiotto, F.; McMaster, J.; Schröder, M. In *Molecular Solar Fuels;* Wydrzynski, T., Hillier, W., Eds.; RSC: Cambridge, U.K., 2011; pp 326−86.
(8) (a) Streich, D.; Astuti, Y.; Orlandi, M.; Schwartz, L.; Lomoth, R.; Hammarström, L.; Ott, S. *Chem. - Eur. J.* **2010**, *16*, 60−63. (b) Zhang, P.; Wang, M.; Na, Y.; Li, X. Q.; Jiang, Y.; Sun, L. C. *Dalton Trans.* **2010**, *39*, 1204−06. (c) Wang, H. Y.; Wang, W. G.; Si, G.; Wang, F.; Tung, C. H.; Wu, L. Z. *Langmuir* **2010**, *26*, 9766−71.
(9) (a) Bingaman, J. L.; Kohnhorst, C. L.; Van Meter, G. A.; McElroy, B. A.; Rakowski, E. A.; Caplins, B. W.; Gutowski, T. A.; Stromberg, C. J.; Webster, C. E.; Heilweil, E. J. *J. Phys. Chem. A* **2012**, *116*, 7261−71. (b) Frederix, P. W. J. M.; Adamczyk, K.; Wright, J. A.; Tuttle, T.; Ulijn, R. V.; Pickett, C. J.; Hunt, N. T. *Organometallics* **2014**, *33*, 5888−96. (c) Kania, R.; Frederix, P. W. J. M.; Wright, J. A.; Ulijn, R. V.; Pickett, C. J.; Hunt, N. T. *J. Chem. Phys.* **2012**, *136*, 044521. (d) Ridley, A. R.; Stewart, A. I.; Adamczyk, K.; Ghosh, H. N.; Kerkeni, B.; Guo, Z. X.; Nibbering, E. T. J.; Pickett, C. J.; Hunt, N. T. *Inorg. Chem.* **2008**, *47*, 7453−55. (e) Stewart, A. I.; Wright, J. A.; Greetham, G. M.; Kaziannis, S.; Santabarbara, S.; Towrie, M.; Parker, A. W.; Pickett, C. J.; Hunt, N. T. *Inorg. Chem.* **2010**, *49*, 9563−73.
(10) (a) Wolpher, H.; Borgström, M.; Hammarström, L.; Bergquist, J.; Sundström, V.; Styring, S.; Sun, L. C.; Åkermark, B. *Inorg. Chem. Commun.* **2003**, *6*, 989−91. (b) Ott, S.; Kritikos, M.; Åkermark, B.; Sun, L. C. *Angew. Chem., Int. Ed.* **2003**, *42*, 3285−88. (c) Ott, S.; Borgström, M.; Kritikos, M.; Lomoth, R.; Bergquist, J.; Åkermark, B.; Hammarström, L.; Sun, L. C. *Inorg. Chem.* **2004**, *43*, 4683−92. (d) Ekström, J.; Abrahamsson, M.; Olson, C.; Bergquist, J.; Kaynak, F. B.; Eriksson, L.; Sun, L. C.; Becker, H. C.; Åkermark, B.; Hammarström, L.; Ott, S. *Dalton Trans.* **2006**, 4599−606. (e) Gao, W. M.; Liu, J. H.; Jiang, W. N.; Wang, M.; Weng, L. H.; Åkermark, B.; Sun, L. C. *C. R. Chim.* **2008**, *11*, 915−21. (f) Song, L. C.; Tang, M. Y.; Mei, S. Z.; Huang, J. H.; Hu, Q. M. *Organometallics* **2007**, *26*, 1575−77. (g) Li, X. Q.; Wang, M.; Zhang, S. P.; Pan, J. X.; Na, Y.; Liu, J. H.; Åkermark, B.; Sun, L. C. *J. Phys. Chem. B* **2008**, *112*, 8198−202. (h) Kluwer, A. M.; Kapre, R.; Hartl, F.; Lutz, M.; Spek, A. L.; Brouwer, A. M.; van Leeuwen, P.; Reek, J. N. H. *Proc. Natl. Acad. Sci. U. S. A.* **2009**, *106*, 10460−65. (i) Song, L. C.; Wang, L. X.; Tang, M. Y.; Li, C. G.; Song, H. B.; Hu, Q. M. *Organometallics* **2009**, *28*, 3834−41. (j) Samuel, A. P. S.; Co, D. T.; Stern, C. L.; Wasielewski, M. R. *J. Am. Chem. Soc.* **2010**, *132*, 8813−15. (k) Wang, H. Y.; Si, G.; Cao, W. N.; Wang, W. G.; Li, Z. J.; Wang, F.; Tung, C. H.; Wu, L. Z. *Chem. Commun.* **2011**, *47*, 8406−08. (l) Liu, J. H.; Jiang, W. N. *Dalton Trans.* **2012**, *41*, 9700−07. (m) Cui, H. H.; Hu, M. Q.; Wen, H. M.; Chai, G. L.; Ma, C. B.; Chen, H.; Chen, C. N. *Dalton Trans.* **2012**, *41*, 13899−907. (n) Wang, W. G.; Wang, F.; Wang, H. Y.; Si, G.; Tung, C. H.; Wu, L. Z. *Chem. - Asian J.* **2010**, *5*, 1796−803. (o) Wang, F.; Wang, W. G.; Wang, H. Y.; Si, G.; Tung, C. H.; Wu, L. Z. *ACS Catal.* **2012**, *2*, 407−16.
(11) (a) Na, Y.; Pan, J. X.; Wang, M.; Sun, L. C. *Inorg. Chem.* **2007**, *46*, 3813−15. (b) Li, P.; Amirjalayer, S.; Hartl, F.; Lutz, M.; de Bruin, B.; Becker, R.; Woutersen, S.; Reek, J. N. H. *Inorg. Chem.* **2014**, *53*, 5373−5383.
(12) (a) Summers, P. A.; Dawson, J.; Ghiotto, F.; Hanson-Heine, M. W. D.; Vuong, K. Q.; Davies, E. S.; Sun, X.-Z.; Besley, N. A.; McMaster, J.; George, M. W.; Schröder, M. *Inorg. Chem.* **2014**, *53*, 4430−4439. (b) Perra, A.; Davies, E. S.; Hyde, J. R.; Wang, Q.; McMaster, J.; Schröder, M. *Chem. Commun.* **2006**, 1103−05.
(13) Wrighton, M.; Morse, D. L. *J. Am. Chem. Soc.* **1974**, *96*, 998−1003.
(14) Wang, Q.; Barclay, J. E.; Blake, A. J.; Davies, E. S.; Evans, D. J.; Marr, A. C.; McInnes, E. J. L.; McMaster, J.; Wilson, C.; Schröder, M. *Chem. - Eur. J.* **2004**, *10*, 3384−96.
(15) Reece, S. Y.; Nocera, D. G. *J. Am. Chem. Soc.* **2005**, *127*, 9448−58.
(16) Ko, C.-C.; Ng, C.-O.; Feng, H.; Chu, W.-K. *Dalton Trans.* **2010**, *39*, 6475−82.
(17) *WINEPR SimFonia,* version 1.25; Brüker Analytische Messtechnik GmbH: Karlsruhe, Germany, 1996.
(18) Perra, A.; Wang, Q.; Blake, A. J.; Davies, E. S.; McMaster, J.; Wilson, C.; Schröder, M. *Dalton Trans.* **2009**, 925−31.
(19) (a) Greetham, G. M.; Burgos, P.; Cao, Q.; Clark, I. P.; Codd, P. S.; Farrow, R. C.; George, M. W.; Kogimtzis, M.; Matousek, P.; Parker, A. W.; Pollard, M. R.; Robinson, D. A.; Xin, Z.-J.; Towrie, M. *Appl. Spectrosc.* **2010**, *64*, 1311−19. (b) Calladine, J. A.; Horvath, R.; Davies, A. J.; Wriglesworth, A.; Sun, X.-Z.; George, M. W. *Appl. Spectrosc.* **2015**, *69*, 519−24.
(20) Caspar, J. V.; Meyer, T. J. *J. Phys. Chem.* **1983**, *87*, 952−57.
(21) Zalis, S.; Consani, C.; El Nahhas, A.; Cannizzo, A.; Chergui, M.; Hartl, F.; Vlček, A. *Inorg. Chim. Acta* **2011**, *374*, 578−585.
(22) Nicholson, R. S.; Shain, I. *Anal. Chem.* **1964**, *36*, 706−723.
(23) Lakowicz, J. R. *Principles of Fluorescence Spectroscopy;* Springer: New York, 2006; pp 80−81.
(24) Glyn, P.; Geroge, M. W.; Hodges, P. M.; Turner, J. J. *J. Chem. Soc., Chem. Commun.* **1989**, 1655−57.
(25) Butler, J. M.; George, M. W.; Schoonover, J. R.; Dattelbaum, D. M.; Meyer, T. J. *Coord. Chem. Rev.* **2007**, *251*, 492−514.
(26) George, M. W.; Johnson, F. P. A.; Westwell, J. R.; Hodges, P. M.; Turner, J. J. *J. Chem. Soc., Dalton Trans.* **1993**, 2977−79.
(27) (a) Chan, S. F.; Chou, M.; Creutz, C.; Matsubara, T.; Sutin, N. *J. Am. Chem. Soc.* **1981**, *103*, 369−79. (b) Neshvad, G.; Hoffman, M. Z. *J. Phys. Chem.* **1989**, *93*, 2445−52. (c) Kalyanasundaram, K. *J. Chem. Soc., Faraday Trans. 2* **1986**, *82*, 2401−15. (d) Probst, B.; Rodenberg, A.; Guttentag, M.; Hamm, P.; Alberto, R. *Inorg. Chem.* **2010**, *49*, 6453−60.
(28) Fujita, E.; Muckerman, J. T. *Inorg. Chem.* **2004**, *43*, 7636−47.

DOI: 10.1021/acs.inorgchem.5b01744
Inorg. Chem. 2016, 55, 527−536